

# Efficient control of an autonomous underwater vehicle while accounting for thruster failure

**Thomas Haberkorn**, Université d'Orléans, France, thomas.haberkorn@univ-orleans.fr  
**Monique Chyba, Ryan Smith**, University of Hawaii Manoa, Hawaii/USA, mchyba@math.hawaii.edu,  
ryan@math.hawaii.edu  
**Song K. Choi, Giacomo Marani, Chris Mcleod**, University of Hawaii Manoa, Hawaii/USA,  
schoi@wiliki.eng.hawaii.edu, marani@wiliki.eng.hawaii.edu, mcleod-eng@hotmail.com

## Abstract

*This paper is concerned with the design and implementation of control strategies onto a test-bed vehicle with six degrees-of-freedom. We design our trajectories to be efficient in time and in power consumption. Moreover, we also consider cases when actuator failure can arise and discuss alternate control strategies in this situation. Our calculations are supplemented by experimental results.*

## 1 Introduction

This paper is a continuation of previously published work found in *Chyba et al. (2007b)*, *Chyba et al. (2007c)* and *Chyba et al. (2007d)*. In these papers, we develop the Switching Time Parameterization (STP) algorithm to design trajectories for an underwater vehicle that are efficient with respect to both time and energy consumption. The main characteristic of our algorithm is that it produces trajectories that can be easily implemented onto a test-bed vehicle. Such implementation along with corresponding experimental data are described in the previously cited papers. Here we propose to extend our study further by considering the possibility of actuator failure. For a long term mission, there is indeed a high percentage that one or more actuators will encounter problems during the time the autonomous underwater vehicle is submerged. Such failures may or may not affect the controllability of the vehicle. In the case that the vehicle is still controllable, we do not want abort the mission. This means that we have to design new trajectories which account for the actuator(s) loss. In the scenario that the actuator failure(s) reduces the mobility of the vessel, and hence implies that the vehicle cannot maneuver as previously prescribed, our goal will be to use the working thrusters to safely bring the vehicle to a station where repairs can be done or it can be rescued.

The model that we consider for a rigid body immersed in a viscous incompressible fluid with rotational flow is as follows. See for instance *Chyba et al. (2007a)*, *Chyba et al. (2007c)* for more details. The position and the orientation of the rigid body are identified with an element of the matrix group of rigid displacement  $SE(3)$ :  $(b, R)$  where  $b = (x, y, z)^t \in R^3$  denotes the position vector of the body and  $R \in SO(3)$  is a rotation matrix describing the orientation of the body. The translational and angular velocities in the body-fixed frame are denoted by  $v = (u, v, w)^t$  and  $\Omega = (p, q, r)^t$  respectively. It follows that the kinematic equations of a rigid body are given by:

$$\dot{b} = Rv, \dot{R} = R\hat{\Omega} \quad (1)$$

where the operator  $\hat{\cdot} : R^3 \rightarrow so(3)$  is defined by  $\hat{y}z = y \times z$ ;  $so(3)$  being the space of skew-symmetric matrices.

For the rest of the paper, we assume that the origin of the body-fixed frame is the center of gravity ( $C_G$ ). Moreover, we assume the body to have three planes of symmetry with body axes that coincide with the principal axes of inertia. The kinetic energy of the rigid body is then given by  $T_{body} = \frac{1}{2}\xi^t \mathbb{I} \xi$  where  $\mathbb{I}$  is the inertia matrix and  $\xi = (v, \Omega)$ .

The equations of motion are given by, see *Fossen (1994)*:

$$M\dot{v} = Mv \times \Omega + D_v(v)v + R^t(\rho g^c \mathcal{V} - mg)k + \varphi_v \quad (2)$$

$$J\dot{\Omega} = J\Omega \times \Omega + Mv \times v + D_\Omega(\Omega)\Omega - r_B \times R^t(\rho g^c \mathcal{V} - mg)k + \tau_\Omega \quad (3)$$

where  $M$  and  $J$  account for the mass, inertia and added mass terms,  $D_v(v), D_\Omega(\Omega)$  represent the drag force and momentum, respectively. In these equations,  $r_B$  is the vector from  $C_G$  to the center of buoyancy ( $C_B$ ),  $\rho$  is the fluid density,  $g$  the acceleration of gravity,  $\mathcal{V}$  the volume of fluid displaced by the rigid body and  $k$  the unit vector pointing in the direction of gravity. Finally, the forces  $\varphi_v = (\varphi_{v_1}, \varphi_{v_2}, \varphi_{v_3})^t$  and  $\tau_\Omega = (\tau_{\Omega_1}, \tau_{\Omega_2}, \tau_{\Omega_3})^t$  account for the control.

The test-bed AUV which we use for our experiments is the Omni-Directional Intelligent Navigator (ODIN) which is owned by the Autonomous Systems Laboratory (ASL), College of Engineering at the University of Hawaii (UH). See Figure 1. This test-bed vehicle is thoroughly introduced in *Chyba et al (2007b)*, *Chyba et al. (2007c)*.

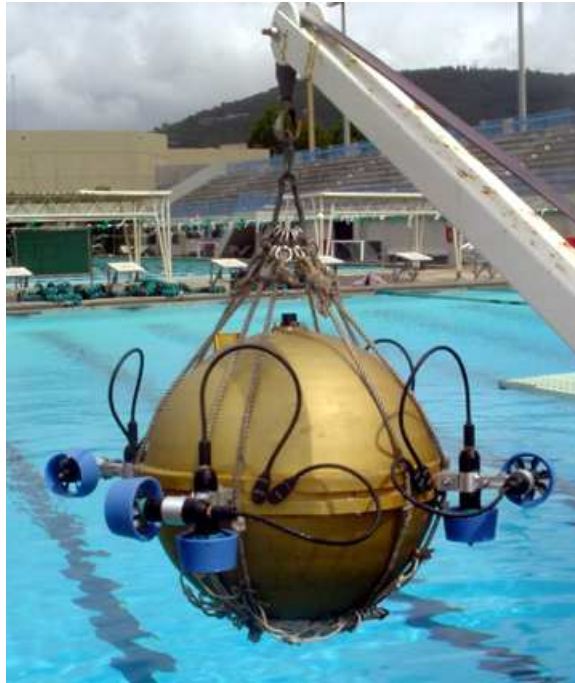


Fig.1: ODIN operating in the pool.

Based on our test-bed vehicle, we assume a diagonal drag force  $D_v(v)$  and a drag momentum  $D_\Omega(\Omega)$ , and our computations for the total drag forces for typical operational velocities suggests a good approximation using a cubic function with no quadratic or constant term. See *Chyba et al. (2007b)*, *Chyba et al. (2007c)* for a justification of this assumption on the drag forces. The hydrodynamics coefficients corresponding to our test-bed vehicle can be found in Table I. These values were derived from experiments performed directly upon ODIN.

$m$	126.55 kg	$\rho g \mathcal{V}$	1243.19 N	$C_B$	(0.49, 0.34, -7) mm
$M_f^u$	70 kg	$M_f^v$	70 kg	$M_f^w$	70 kg
$I_x$	5.46 kg.m <sup>2</sup>	$I_y$	5.29 kg.m <sup>2</sup>	$I_z$	5.72 kg.m <sup>2</sup>
$J_f^p$	0 kg.m <sup>2</sup>	$J_f^q$	0 kg.m <sup>2</sup>	$J_f^r$	0 kg.m <sup>2</sup>
$D_v^{11}$	-27.0273	$D_v^{21}$	-27.0273	$D_v^{31}$	-27.0273
$D_v^{12}$	-897.6553	$D_v^{22}$	-897.6553	$D_v^{32}$	-897.6553
$D_\Omega^{11}$	-13.793	$D_\Omega^{21}$	-13.793	$D_\Omega^{31}$	-11.9424
$D_\Omega^{12}$	-6.4594	$D_\Omega^{22}$	-6.4594	$D_\Omega^{32}$	-6.9393

Table I: Numerical values for hydrodynamic coefficients.

From Figure 1, we clearly see that the forces from the eight thrusters do not act directly at  $C_G$  as assumed.

Also, the control torques are obtained from the moments created by the applied forces of the thrusters. For implementation of control strategies, we must compute the transformation between the computed 6 DOF controls and the eight individual controls for each thruster. First, let us denote  $\gamma_i$ ,  $i = 1, 3, 5, 7$  as the thrusts induced by the horizontal thrusters and  $\gamma_i$ ,  $i = 2, 4, 6, 8$  as the thrusts induced by the vertical thrusters. We assume that the points of application of the thrusts  $\gamma_i^{(h,v)}$  lie in a plane which intersects the center of the spherical body of ODIN. We also assume that the distance from the center of the body-fixed reference frame ( $C_G$ ) to  $C_B$  is small with respect to the radius of the sphere. This later assumption allows us to decouple the actions of the thrusters. Hence, the horizontal thrusters contribute only to the forces  $\varphi_{v_1}$  (surge) and  $\varphi_{v_2}$  (sway) and to the torque  $\tau_{\Omega_3}$  (yaw). The vertical thrusters contribute only to the force  $\varphi_{v_3}$  (heave) and to the torques  $\tau_{\Omega_1}$  (roll) and  $\tau_{\Omega_2}$  (pitch). Under these assumptions, we are able to determine that the linear transformation from the 6 DOF controls to the 8 dimensional thruster controls is given by  $(\varphi, \tau) = TCM \cdot \gamma$ . Here TCM stands for Thrust Conversion Matrix, and is given by:

$$TCM = \begin{pmatrix} -e_1 & 0 & e_1 & 0 & e_1 & 0 & -e_1 & 0 \\ e_1 & 0 & e_1 & 0 & -e_1 & 0 & -e_1 & 0 \\ 0 & -1 & 0 & -1 & 0 & -1 & 0 & -1 \\ 0 & -e_3 & 0 & -e_3 & 0 & e_3 & 0 & e_3 \\ 0 & e_3 & 0 & -e_3 & 0 & -e_3 & 0 & e_3 \\ e_2 & 0 & -e_2 & 0 & e_2 & 0 & -e_2 & 0 \end{pmatrix} \quad (4)$$

for  $e_1 = 0.7071$ ,  $e_2 = 0.4816$  and  $e_3 = -0.2699$ .

ODIN's thrusters are independently powered and we can reasonably state that each thrust  $\gamma_i$  is bounded by fixed values:

$$\gamma \in \Gamma = \{\gamma \in \mathbf{R}^8 | \gamma_i^{\min} \leq \gamma_i \leq \gamma_i^{\max}, i = 1, \dots, 8\}. \quad (5)$$

Based on this design, the power consumption criterion is directly related to the action of each thruster, and is described in detail in section 2.1. The bounding thrust values for each thruster were determined through experimentation are are found in Table II.

$\gamma_1^{\min}$	-14.1098 N	$\gamma_1^{\max}$	4.8706 N	$\gamma_5^{\min}$	-13.8294 N	$\gamma_5^{\max}$	7.2806 N
$\gamma_2^{\min}$	-10.9051 N	$\gamma_2^{\max}$	5.4818 N	$\gamma_6^{\min}$	-14.6013 N	$\gamma_6^{\max}$	5.1035 N
$\gamma_3^{\min}$	-18.5574 N	$\gamma_3^{\max}$	7.1596 N	$\gamma_7^{\min}$	-13.3303 N	$\gamma_7^{\max}$	6.2808 N
$\gamma_4^{\min}$	-13.3118 N	$\gamma_4^{\max}$	7.3392 N	$\gamma_8^{\min}$	-14.4213 N	$\gamma_8^{\max}$	5.7958 N

Table II: Maximum and minimum bounds for each of ODIN's thrusters.

## 2 Criteria and Maximum Principle

In this section we define the criteria that we consider for minimization and we apply the necessary condition of the Pontryagin Maximum Principle (PMP) to the underlying optimal control problems (OCP) in order to get insights on the structures of the optimal trajectories. Finally, we include scenarii involving one or several thruster failure.

### 2.1 Criteria

One of the main issue in designing an AUV it to maximize its autonomy. However, we usually do not want at the same time expand too much the duration of the trajectories. Hence, our goal is to minimize a combination of both the time and the power consumption.

Our approach to reach that goal is the following. We first study the minimum time problem. Then, based on the optimal time duration to steer our vehicle from a set of given initial and final positions at rest we study the minimum power consumption problem. The power consumption criterion considered here is based on our test-bed vehicle introduced earlier. ODIN is powered by on-board batteries, hence its

autonomy is directly affected by the lifespan of those batteries. Hence in order to increase the vehicle's autonomy, we need to design trajectories for which the thruster's power consumption is reduced as to a minimum.

Since a minimum time trajectory will use all the thruster power available to quickly reach the final configuration, we cannot expect a time optimal trajectory to be efficient with respect to power consumption. We must then determine the quantity of power consumption that we can save by increasing the time duration to reach the final configuration from the minimum time. This question is addressed in the section 2.5 where we give some numerical results to support our answer. Of course, the ultimate goal is to find a good balance between the minimum time and the minimum power consumption one but this depends not only on the vehicle but also on the mission it has to accomplish.

Let us now describe mathematically the power consumption criterion. ODIN is actuated by eight thrusters that are powered by 20 batteries. Each thruster is powered by a constant voltage and pulls as much current as necessary to deliver a specific thrust. The on-board electronics required far less power than the thrusters and are supplied by a set of 4 batteries that will always outlive the ones of the thrusters. Thus, minimizing the power consumption for a given trajectory is equivalent to the minimization of the current pulled by the thrusters during this trajectory. To model our criterion, we performed individual thruster experiments to relate the delivered thrust to the pulled current. We tested each thruster four times through its operational thrust range and recorded the thrust as well as the pulled current. We averaged the relation for each thruster. Little to no variation of this relation with respect to different thrusters was observed. We choose the following relation:

$$Amps(\gamma_i) = \begin{cases} -0.4433\gamma_i & = \alpha_- \gamma_i, \text{ if } \gamma_i \leq 0 \\ 0.2561\gamma_i & = \alpha_+ \gamma_i, \text{ if } \gamma_i \geq 0 \end{cases}, \text{ for } i = 1, \dots, 8 \quad (6)$$

where  $Amps(\gamma_i)$  (A) is the current pulled when thrust  $\gamma_i$  (N) is applied by the  $i^{th}$  thruster. The relation is the same for each thruster. Note that it is not symmetric, since the thrusters have a preferred direction of thrust due to the design of the propeller's shaft. The lifespan of a battery being measured in A.h, we write the power consumption criterion of all the thrusters as:

$$C(\gamma) = \int_0^T \sum_{i=1}^8 Amps(\gamma_i(t)) dt, \quad (7)$$

where the final time  $T$  can either be fixed or be part of the optimization process. If we do not fix the final time *a priori*, we can still expect a finite time. This is a consequence of the fact that ODIN is positively buoyant, hence a nonzero power is constantly needed to overcome the buoyancy force which makes long duration trajectories non efficient. Notice that assuming a free final time induces additional numerical difficulties. Moreover, we are interested in the variation of the consumption with respect to the time duration allowed for the trajectory. For those reasons, we decide to fix the final time and only then optimize the trajectory with respect to our  $C(\gamma)$  criterion.

To set the final time, it is natural to use the knowledge of the minimum time required to reach the final configuration  $\chi_T$ . This minimum time corresponds to the solution of the time minimum problem, we denote it by  $T_{\min}$ . We then set the fixed final time  $T$  to a multiple  $c_T$  of  $T_{\min}$ :

$$T = c_T \cdot T_{\min}, c_T \geq 1. \quad (8)$$

Note that if  $c_T < 1$ , then the problem does not have a solution. If  $c_T = 1$ , then the minimum time and minimum consumption problems provide the same solution. In section 2.5, we show the evolution of the consumption as  $c_T$  increases. From now on, we denote by  $C_{c_T}$  the optimal power consumption  $C(\gamma)$  for  $T = c_T \cdot T_{\min}$ .

## 2.2 Maximum Principle

The maximum principle, *Pontryagin et al. (1968)*, is a powerful mathematical tool in optimal control theory. It gives necessary conditions for a control strategy and its corresponding trajectory to be optimal. Although we will not directly use those conditions in the design of our trajectories, we discuss them to introduce the notion of bang-bang and singular arcs as well as to justify our numeric choices for the STP algorithm.

We denote by  $\chi = (\eta, v, \Omega)^t$  a configuration for the vehicle and let us consider the optimal control problem of steering our AUV from  $\chi_0$  to  $\chi_T$ , while minimizing a given integral cost  $\int_0^T l(\chi(t), \gamma(t))dt$ .

To apply the maximum principle, we introduce the following Hamiltonian function  $H$ :

$$H(\chi, \lambda, \gamma) = -\lambda_0 l(\chi, \gamma) + \lambda^t \dot{\chi}(\chi, \gamma), \quad (9)$$

where  $\lambda_0$  is a constant that can be normalized to 0 or 1,  $\lambda = (\lambda_\eta, \lambda_{nv}, \lambda_\Omega)$  is a vector function in  $\mathbf{R}^{12}$  called the adjoint vector, and  $\dot{\chi}(\chi, \gamma)$  is given by the equations of motion 3.

Assume that there exists an admissible optimal control  $\gamma : [0, T] \mapsto \Gamma$ , such that the corresponding trajectory  $\chi : [0, T] \mapsto \mathbf{R}^{12}$  steers the vehicle from  $\chi_0$  to  $\chi_T$ . Then, the maximum principle tells us that there exist an absolutely continuous adjoint vector  $\lambda : [0, T] \mapsto \mathbf{R}^{12}$ ,  $(\lambda, \lambda_0) \neq 0$  such that  $\chi$  and  $\lambda$  are solutions almost everywhere (a.e.) on  $[0, T]$  of:

$$\dot{\chi} = \frac{\partial H}{\partial \lambda}, \quad \dot{\lambda} = -\frac{\partial H}{\partial \chi}, \quad (10)$$

and such that the maximum condition holds:

$$H(\chi(t), \lambda(t), \gamma(t)) = \sup_{u \in \Gamma} H(\chi(t), \lambda(t), u), \quad a.e. \text{ on } [0, T] \quad (11)$$

In the case the final time  $T$  is free, we add the condition  $H(\chi(t), \lambda(t), \gamma(t)) = 0$ . A triple  $(\chi, \lambda, \gamma)$  that satisfies the maximum principle is called an extremal.

As will be seen in the next section, the functions  $\kappa_i$ ,  $i = 1, \dots, 8$  defined as the multiplying coefficients of  $\gamma_i$  in  $H$  plays a crucial in the structure of optimal strategies. In other words  $\kappa_i$  is the  $i^{\text{th}}$  column of the vector  $(\lambda_\gamma, \lambda_\Omega)^t TCM(M^{-1}, J^{-1})$ . For instance:

$$\kappa_1 = -\frac{e_1 \lambda_{v_1}}{m_1} + \frac{e_1 \lambda_{v_2}}{m_2} + \frac{e_2 \lambda_{\Omega_3}}{I_3} \quad (12)$$

## 2.3 Time minimization

We already studied the time minimization in previous papers such as *Chyba et al. (2007b) and (2007c)*. However, in these papers the optimization was taken over the 6 DOF control  $(\varphi, \tau)$  and not the real applied controls  $\gamma_i$ . For the eight dimensional control we are using a larger control domain which implies smaller minimum time but also different shapes of optimal control strategies. Additionally, we are not assuming the same bounds hold for each thrusters, as we did in *Chyba et al. (2007c)*.

Let us briefly describe our results. The time criterion corresponds to the integral cost  $l(\chi, \gamma) = 1$  with free final time  $T$ . In this case, the maximum condition (11) implies that an optimal control  $\gamma$  satisfies the following relations:

$$\gamma_i = \begin{cases} \gamma_i^{\min} & , \text{ if } \kappa_i < 0 \\ \in [\gamma_i^{\min}, \gamma_i^{\max}] & , \text{ if } \kappa_i = 0 \\ \gamma_i^{\max} & , \text{ if } \kappa_i > 0 \end{cases}, \quad i = 1, \dots, 8. \quad (13)$$

So the zeros of  $\kappa_i$  determine the structure of the optimal control strategy, we call these functions the switching functions. from the maximum principle we have that for  $\kappa_i \neq 0$  a.e. on  $[0, T]$  the optimal control  $\gamma_i$  takes its values in  $\{\gamma_i^{\min}, \gamma_i^{\max}\}$  a.e. In such a case, the control  $\gamma_i$  is said to be bang-bang. If,

on the contrary, there exists a nontrivial time interval  $[t_1, t_2] \subset [0, T]$  such that  $\kappa_i$  vanishes on  $[t_1, t_2]$ , the control cannot be deduced directly from the maximum principle. In this case, we call the control singular on  $[t_1, t_2]$ . A time at which  $\kappa_i$  changes sign or vanishes with a nonzero derivative is called a switching time. Practically, a switching corresponds either to  $\gamma_i$  discontinuous and jumping from one bound to the other (e.g. from  $\gamma_i^{\min}$  to  $\gamma_i^{\max}$ ) either to a change from singular to bang (or from bang to singular). A theoretical study for the search of the optimal solution is extremely, if not impossible, complicated. For this reason we use numerical computations.

Discretizing the (OCP) along the state  $\chi$  and the control  $\gamma$ , we can transform it into a nonlinear programming problem (NLP). This (NLP) can then be solved by a standard large scale nonlinear optimization solver. We use *Ampl*, see *Fourer et al. (1993)*, to model the (NLP) and *IpOpt*, see *Wächter and Biegler (2006)*, to solve it. The discretization scheme is a second order Runge-Kutta and the optimization parameters are the discretized state and control as well as the final time we wish to minimize. On a 2Ghz Pentium M processor with 2 Go of RAM, the solving of such a problem with 1000 discretization steps (thus with  $\approx (12 + 8) \times 1000 = 20000$  optimization parameters) takes about 20 min to converge without any clever initialization.

Figure 2 shows a solution. The initial configuration is the origin at rest ( $\chi_0 = (0, \dots, 0)$ ) and the final configuration is taken as  $\chi_T = (5, 4, 1, 0, \dots, 0)$ .

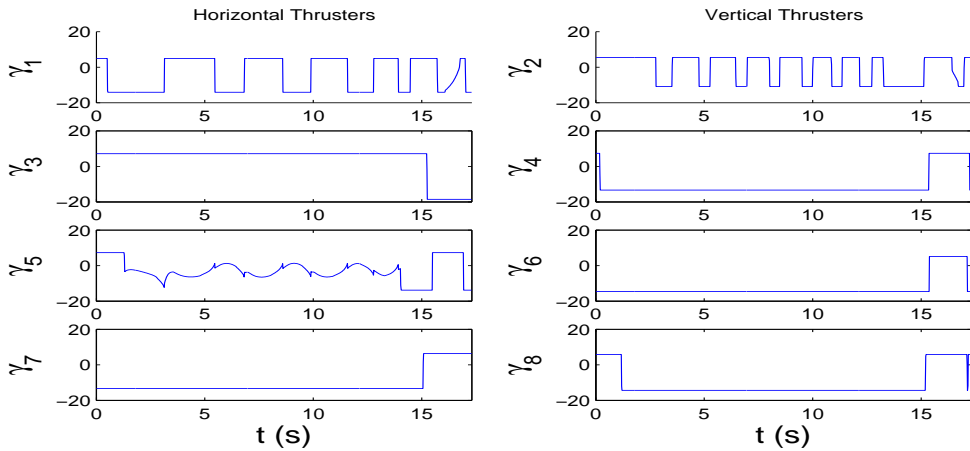


Fig.2: Minimum time optimal control strategy for  $\chi_T = (5, 4, 1, 0, \dots, 0)$ :  $T_{\min} \approx 17.3083s$ .

For this final configuration, the computed minimum time is  $T_{\min} \approx 17.3083s$ . In Figure 2, one can see that most of the controls are bang-bang except for  $\gamma_5$  which is mainly singular. This is in accordance with the maximum principle. If we use the Lagrange multipliers of the optimization, which are actually the discretized adjoint vector (up to a sign), we see that  $\gamma$  satisfies the maximum condition (13). One should note that  $\gamma_5$  is one of the horizontal thrusters and that its singularity corresponds to a need for a fine Yaw control  $\tau_{\Omega_3}$ . As expected, the use of thruster level is nearly maximum which leads to a high power consumption, here we have  $C_1 \approx 571.5548 A.s$ . Similar to previous observation on the minimum time problem with the 6 DOF control, such a control strategy is not implementable on our test-bed AUV. Indeed, there are too many thruster's changes for the bang-bang arcs and the control varies continuously along the singular arc which cannot be implemented in practice. We will see in a future section how to address these issues with the STP algorithm.

## 2.4 Consumption minimization

When considering the power consumption criterion, the integral cost corresponds to  $l(\chi, \gamma) = \sum_{i=1}^8 Amps(\gamma_i)$  and  $T$  is fixed to a multiple of  $T_{\min}$ . Contrary to the time this energy like criterion depends directly on the control  $\gamma$ . As a consequence, the maximization condition (11) depends on the value of the constant  $\lambda_0$  (0 or 1) and a thorough analysis of the 2 cases should be conducted. However, we are

here interested in applicable solutions and will eventually design our trajectories using our STP algorithm that does not rely on the maximum principle. For this reason we omit such analysis in this paper and directly assume that  $\lambda_0 = 1$  (the normal case). In this case, the maximization condition (11) implies that the control  $\gamma$  satisfies:

$$\gamma_i = \begin{cases} \gamma_i^{\min} & , \text{ if } \kappa_i < \alpha_- \\ \in [\gamma_i^{\min}, 0] & , \text{ if } \kappa_i = \alpha_- \\ 0 & , \text{ if } \kappa_i \in (\alpha_-, \alpha_+) \\ \in [0, \gamma_i^{\max}] & , \text{ if } \kappa_i = \alpha_+ \\ \gamma_i^{\max} & , \text{ if } \kappa_i > \alpha_+ \end{cases} \quad i = 1, \dots, 8. \quad (14)$$

Here, if  $\kappa_i$  is not equal to  $\alpha_-$  or  $\alpha_+$ , the control  $\gamma_i$  takes its values in  $\{\gamma_i^{\min}, 0, \gamma_i^{\max}\}$ . If  $\kappa_i$  is equal to  $\alpha_-$  or  $\alpha_+$  on a nontrivial interval  $[t_1, t_2] \subset [0, T]$ , then the control  $\gamma_i$  is said to be singular. A switching time is then defined as for the minimum time case.

Since the  $\kappa_i$  are linear combinations of the components of the absolutely continuous adjoint vector  $\lambda$ , we know that the value 0 will play a major role in the optimization. observe that our criterion is not differentiable for  $\gamma_i = 0$ , we then must rewrite it in order to be able to apply our numerical method. Indeed, most nonlinear optimization solvers require the constraints and the criterion to be a least twice differentiable. To overcome this difficulty, we use a standard numerical idea that consists in splitting each control  $\gamma_i$  in its negative ( $\gamma_i^- = \min(\gamma_i, 0)$ ) and positive ( $\gamma_i^+ = \max(\gamma_i, 0)$ ) parts. Then  $\gamma_i = \gamma_i^- + \gamma_i^+$ ,  $\gamma_i^- \in [\gamma_i^{\min}, 0]$  and  $\gamma_i^+ \in [0, \gamma_i^{\max}]$ . The consumption criterion becomes:

$$C(\gamma) = \int_0^T \sum_{i=1}^8 \alpha_- \gamma_i^-(t) + \alpha_+ \gamma_i^+(t) dt, \quad (15)$$

which is smooth with respect to  $\gamma_i^-$  and  $\gamma_i^+$ . We can now apply the same numerical method as for the minimum time, the only differences being the criterion and the splitting of the discretized controls, so the number of optimization parameters for  $\gamma$  is doubled.

In Figure 3, we show minimum consumption control strategies for  $c_T = 1.5, 2$  and  $2.5$ . The terminal configuration is the same as for the previous minimum time solution. For comparison issues, the duration of the trajectories have been rescaled to  $[0, 1]$ .

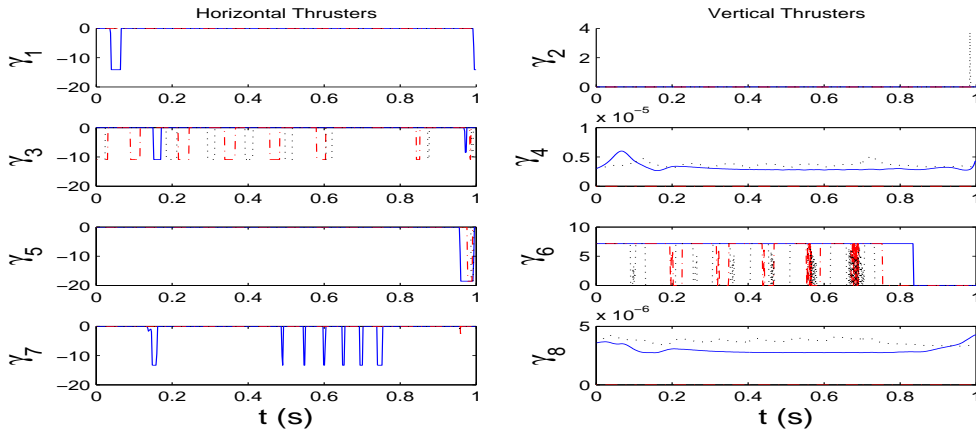


Fig.3: Minimum consumption control strategies for  $c_T = 1.5$  (plain),  $2$  (dashed) and  $2.5$  (dotted) and for  $\chi_T = (5, 4, 1, 0, \dots, 0)$ .

In Figure 3, we see that as expected from the maximum principle, the control strategies are piecewise constant and take their values in  $\{\gamma_i^{\min}, 0, \gamma_i^{\max}\}$ . The controls  $\gamma_4$  and  $\gamma_8$  are numerically equal to zero since their magnitude is approximatively  $10^{-5}$ . We also see that the more time we allow for the trajectory, the

more zero thrust arcs we have. This is clearly reflected by the value of the criteria:  $C_{1.5} \approx 211.9413 > C_{2.0} \approx 160.6891 > C_{2.5} \approx 151.5259$  A.s. When compared to the consumption of the minimum time solution ( $C_1 \approx 571.5548$  A.s), we see that simply allowing 50% more time for the trajectory leads to a consumption saving of more than 60%. We will see in section 2.5 precisely how evolves the criterion with respect to  $c_T$ .

As for the minimum time control strategies, the minimum consumption control strategies are clearly not implementable on our test-bed AUV. Indeed, the number of discontinuities of the control is too large and some discontinuities are too close to each other to be safely realized by a real thruster. That's why we will adapt the algorithm already described in *Chyba et al. (2007b) and (2007c)* to the design of consumption efficient and implementable control strategies. But first, we will take a quick look at the thruster failure case.

## 2.5 Thruster Failure

Our AUV is actuated by 8 thrusters evenly distributed around its circumference. Since we only have 6 DOF, we see that we have some actuator redundancies. A natural question is to know exactly how many thrusters we really need to reach a given final configuration. Controllability issues when facing a smaller number of actuator available are currently under investigations. In this paper, we will discuss some cases in which the loss of one or more thrusters is not detrimental to the controllability of the vehicle.

We restrict ourself to final configurations  $\chi_0$  and  $\chi_T$  at rest with no inclinations. In *Chyba et al. (2007b)*, we present a basic method to design control strategies that steers  $\chi_0$  to  $\chi_T$ . This method is based on the decomposition of the trajectory into pure motions along one of the vehicle axis of inertia. Imagine one wants to steer the AUV from the origin to a final configuration  $\chi_T = (x_T, y_T, z_T, 0, \dots, 0)$ . Then one can do it by first applying a pure Surge control acceleration then deceleration  $\varphi_{v_1}$  till reaching  $\chi_1 = (x_f, 0, \dots, 0)$ . Then one will continue by a pure Sway acceleration and deceleration and finally a pure Heave acceleration then deceleration.

So in order to be able to reach a straight final configuration at rest, it is enough to be able to apply pure Surge, Sway and Heave. There is simply one adjustment to do since one also needs to compensate the positive buoyancy along each pure motion. So as long as the 6 DOF control domain  $\mathcal{U} = TCM \cdot \Gamma$  contains an interval of the form  $[-\epsilon, \epsilon]^2 \times [B - mg - \epsilon, B - mg + \epsilon] \times \{0\}^3$ ,  $\epsilon > 0$ , it is possible to steer the AUV from one straight configuration at rest to another. Of course, this is only a sufficient condition since other trajectories are available.

With this first result, we can already conclude that since the horizontal thrusters only contribute to  $\varphi_{v_1}, \varphi_{v_2}$  and  $\tau_{\Omega_3}$  and the vertical only contributes to  $\varphi_{v_3}, \tau_{\Omega_1}$  and  $\tau_{\Omega_2}$ , the following thruster failures do not hinder the AUV capability of joining the desired configurations:

- the loss of one horizontal ( $\gamma_{1,3,5,7}$ ) and one vertical thruster ( $\gamma_{2,4,6,8}$ ).
- the loss of one horizontal thruster and two opposite vertical thrusters ( $(\gamma_2, \gamma_6)$  or  $(\gamma_4, \gamma_8)$ ).

Depending on which thrusters we lose, we might still be able to design trajectories. We can even lose three thrusters ( $\gamma_1, \gamma_2$  and  $\gamma_6$  for example) and still be controllable.

Based on the fact that some thruster failure scenarii do not prevent us from reaching a given  $\chi_T$ , we can apply the numerical methods used before with a slight adaptation that consist in adding constraints stating that one or more thrusts have to be identically zero. Table III gives the computed minimum time and corresponding consumption for various thruster failure scenarii. The initial configuration is the origin and the final one is  $\chi_T = (5, 4, 1, 0, \dots, 0)$ .

Looking at the fully actuated control strategies of Figure 3, we see that some thrusters were barely used when minimizing the consumption. Actually only controls  $\gamma_3, \gamma_6$  and  $\gamma_7$  seem to be really useful for the optimal consumption strategy. In Table III, if we only consider the scenarii with one thruster failure, we



Failure	$T_{\min}$ (s)	$C_1$ (A.s)	Failure	$T_{\min}$ (s)	$C_1$ (A.s)
None	17.3083	571.5548	{8}	18.0720	519.0309
{1}	17.6877	540.3961	{2, 5}	18.0089	499.8542
{2}	17.4860	536.4475	{5, 6}	21.5692	497.2662
{3}	18.4164	559.7070	{6, 7}	20.0594	547.2247
{4}	18.0367	524.4966	{1, 2, 6}	22.1338	533.5479
{5}	17.5873	546.7636	{2, 5, 6}	23.0075	448.8605
{6}	19.2788	562.2535	{4, 5, 8}	20.3499	421.3308
{7}	18.5035	598.5646	{6, 7, 8}	22.3533	586.4943

Table III: *Minimum time and corresponding consumption for  $\chi_T = (5, 4, 1, 0, \dots, 0)$  and thruster failure scenarii.*

see that it is precisely when the *consumption useful* controls fail that the minimum time is increased the most. All the less used thrusters give minimum final time really close to the fully actuated scenario.

When looking at scenarii with two thruster failures, we see that the {2, 5} one gives a minimum time even better than the single failure of thrusters 3, 6 or 7. The loss of the pairs {5, 6} or {6, 7} yields a final time greater than any of the single loss cases, which was expected. Finally, looking at the worst failure scenarii, where we lose the ability to use three thrusters, we see that the scenario {4, 5, 8}, which corresponds to thrusters barely used in the fully actuated minimum consumption strategy, yields a fairly good minimum time, when compared to the others 3 failure scenarii. Overall, those results suggests that the fully actuated minimum time control strategy is a good indicators of which thrusters we can lose without alteratin the AUV's performance too much. Of course, this depends heavily on the considered terminal configuration. For instance, if we take  $\chi_T = (-5, -4, -1, 0, \dots, 0)$  we can expect another hierarchy of the thrusters.

Because more than the minimum time needed to reach a given  $\chi_T$  in case of actuator failure, it is interesting to study the impact of various thruster failure scenarii on the minimum power consumption problem. Figure 4 shows the evolution, for various thruster failure scenarii, of the consumption criterion with respect to  $c_T$ . Here,  $c_T$  refers to the multiplying coefficient applied to the  $T_{\min}$  of the fully actuated case, which explains that none of the curve except one, are starting at  $c_T = 1$ .

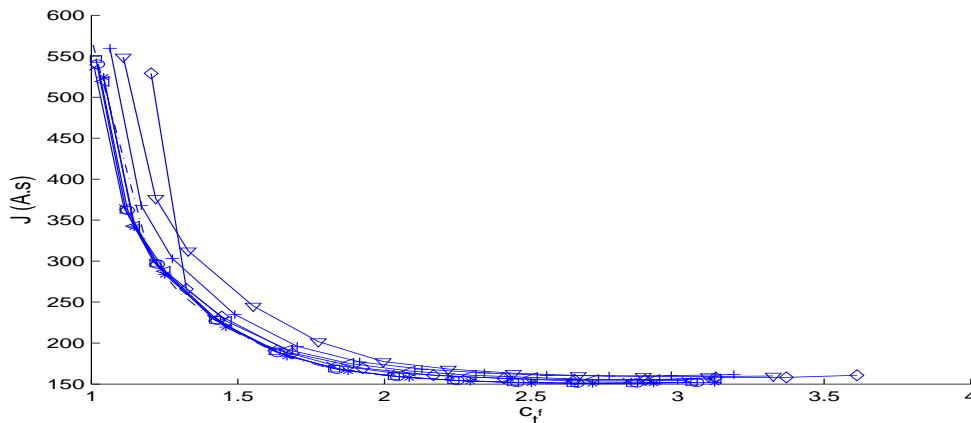


Fig.4: *Consumption evolutions for various thruster failure scenarii and  $\chi_T = (5, 4, 1, 0, \dots, 0)$ .*

In Figure 4, we see that the evolution trend of the consumption with respect to  $c_T$  is pretty similar for all the thruster scenarii. The best evolution, that is the one below all the other, is of course the one corresponding to the fully actuated case. As expected, the 2 thrusters failure scenarii are less consumption efficient than the one thruster failure and the 3 thrusters failure are less consumption efficient than the 2 thrusters failure. From a pure consumption point of view, the most important aspect of those evolutions is that we can save a lot of power by allowing more time to perform the trajectory. Also, the consumption

evolution is first decreasing and then starts to increase after  $c_T \approx 2.80$ . This is due to the dissipative characteristic of our mechanical system, represented by the positive buoyancy. So we know for sure that a minimization of the consumption with a free final time will yield a finite time, provided the numerical solving converges. Quantitatively speaking, the best consumption is usually nearly a quarter of the minimum time consumption ( $\approx 160 A.s$  vs.  $\approx 570 A.s$ ). However, the power saving decreases when losing thrusters, which is completely natural since we reduce the control domain  $\Gamma$  and thus can only perform less effectively.

### 3 Consumption and Switching Time Parameterization

From the previous numerical results, we can easily conclude that the autonomy of our AUV can be easily improved by allowing a slightly longer trajectory duration than the minimum one. This is still the case when facing thrusters failure. However, clearly the trajectories designed in the previous sections are not implementable on a real vehicle. To remedy to that we use a similar idea to the one used in *Chyba et al. (2007b)* and *Chyba et al (2007c)*, the so called Switching Time Parameterization Problem (*STPP*). We rewrite the (*OCP*) into a particular (*NLP*). This (*NLP*), called (*STPP*), is a discretization of the (*OCP*) where the control strategy is set to be piecewise constant with only a small number of discontinuities. This small number of discontinuities will prevent the computation of un-implementable control strategy. Let  $p$  be the number of allowed times at which one or several controls are discontinuous. Then, our new nonlinear programming problem is:

$$(STPP)_p \begin{cases} \min_{z \in \mathcal{D}} \sum_{i=1}^p \sum_{j=1}^8 (\alpha_- \gamma_{j,i}^- + \alpha_+ \gamma_{j,i}^+) \\ t_0 = 0, t_{p+1} = T \\ t_{i+1} = t_i + \xi_i, i = 1, \dots, p \\ \chi_{i+1} = \chi_i + \int_{t_i}^{t_{i+1}} \dot{\chi}(t, \gamma_i^- + \gamma_i^+) dt \\ \chi_{p+1} = \chi_T \\ z = (\xi_1, \dots, \xi_{p+1}, \gamma_1^-, \gamma_1^+, \dots, \gamma_{p+1}^-, \gamma_{p+1}^+) \\ \mathcal{D} = \mathbf{R}_+^{(p+1)} \times (\Gamma^- \times \Gamma^+)^{(p+1)} \end{cases} \quad (16)$$

where  $\xi_i, i = 1, \dots, p+1$  are the time arclengths and  $(\gamma_i^- + \gamma_i^+) \in \Gamma, i = 1, \dots, p+1$  are the negative and positive parts of the constant thrust arcs.  $\dot{\chi}(t, \gamma_i^-, \gamma_i^+)$  is the right hand side of the dynamic system (1), (2) and (3) with the constant thrust  $\gamma_i^- + \gamma_i^+$ .

Actually, a solution of the  $(STPP)_p$  problem would still not be implementable because discontinuities of the control strategy would damage the thrusters. Thus, we rewrite again  $(STPP)_p$  and add linear junctions instead of discontinuities. Doing so, we know that a solution of the smoothed  $(STPP)_p$ , still called  $(STPP)_p$ , will have smooth transitions from one constant thrust to the other.

To solve this problem, we again use *Ampl* for the modeling and *IpOpt* for the solving. Note that we discretize the dynamic constraint ( $\chi_{i+1} = \chi_i + \int_{t_i}^{t_{i+1}} \dot{\chi} dt$ ) using a second order Runge-Kutta scheme. This means that contrary to the approach used in our previous papers, we don't use a high order integrator to compute this constraint. Additionally, this discretization forces us to consider the discretized state to be part of the optimization process. Thus, this  $(STPP)_p$  implementation requires more computational resources than the one of *Chyba et al. (2007b)* and *Chyba et al. (2007c)*. However, this is compensated by the fact that adding more optimization parameters and constraints helps the solver to converge faster and also gets rid of many local minima we were encountering before. The reason behind our second discretization is that a straight numerical implementation of  $(STPP)_p$ , when considering thruster failure, appeared to be way too sensitive to the initialization and to the accuracy of the Jacobian evaluation of the constraints. Nevertheless, the discretized  $(STPP)_p$  has no convergence issue and we can easily and rapidly compute  $(STPP)_p$  solutions. Note however that we still encounter some local minima that are easily spotted since they yield inconsistent consumption values.

Table IV summarizes minimum consumption results for the  $(STPP)_2$  problem and for various thruster failure scenarios. Note that the final configuration is again  $\chi_T = (5, 4, 1, 0, \dots, 0)$  and that the  $c_T$  coefficient always refers to the fully actuated minimum time, so  $T = c_T \cdot 17.3083 s$ .

Failure	$C_{1.5}$ (A.s)	$C_2$ (A.s)	$C_{2.5}$ (A.s)	Failure	$C_{1.5}$ (A.s)	$C_2$ (A.s)	$C_{2.5}$ (A.s)
None	236.5387	173.8771	163.0436	{2, 5}	237.4845	179.3836	167.9275
{1}	236.9052	175.3976	164.2833	{5, 6}	315.6937	174.6172	163.7441
{3}	382.4933	290.1979	NCV	{6, 7}	$< T_{\min}^{STPP_2}$	321.9383	234.5945
{4}	237.8894	173.8829	163.0442	{1, 2, 6}	$< T_{\min}^{STPP_2}$	180.1765	168.3649
{6}	298.7540	173.8846	163.3044	{2, 5, 6}	358.9615	179.5259	167.9275
{7}	356.5089	240.3102	211.3583	{4, 5, 8}	246.7363	174.8636	163.7440

Table IV:  $(STPP)_2$  consumptions for  $\chi_T = (5, 4, 1, 0, \dots, 0)$  and various  $c_T$  and thruster failure scenarii.

As for the  $(STTP)$  method applied to the fully actuated minimum time and minimum consumption cases, the results of Table IV are very good when compared to Figure 4. Indeed, we see that while designing implementable control strategy, we do not lose much efficiency in terms of power consumption. However, a careful look at the table indicate that for some thruster failure scenarii, there seems to be a large difference of efficiency. For instance, when thrusters {6, 7} fail, we see that the  $C_2$  optimal consumption is nearly twice the one of for some other scenarii. This is mainly due to the fact that the  $(STPP)_2$  minimum time  $T_{\min}^{STPP_2}$  is quite high since in this specific case it is 33.2362 s. So, since the multiplying coefficient is applied to the fully actuated minimum time  $T_{\min}$ , we see that allowing the {6, 7} scenario twice  $T_{\min}$  actually gives very little additional time. For other less efficient scenarii, like {3}, the problem does not come from a large  $T_{\min}^{STPP_2}$  but probably from the drastic reduction of the admissible control strategy.

Figure 5 shows the thrust strategy solution of  $(STPP)_2$  when thrusters {4, 5, 8} are not used. The  $c_T$  is taken as 2 and the final configuration is the usual one.

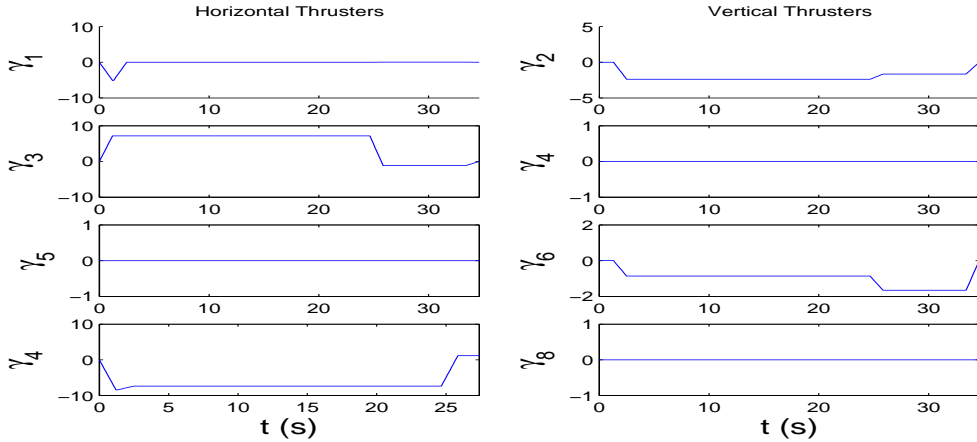


Fig.5:  $(STPP)_2$  control strategy for  $\chi_T = (5, 4, 1, 0, \dots, 0)$ ,  $c_T = 2$  and loss of thrusters {4, 5, 8}.

On Figure 5, we can see that we are not using the controls  $\gamma_4$ ,  $\gamma_5$  and  $\gamma_8$ , so we are respecting the thruster failure scenario. Moreover, the active control clearly exhibit a piecewise constant structure with linear junctions instead of discontinuities. Note that the length of the linear junctions has been set to 1.2 s. The first constant thrust arc is very small, which explains why there is a peak on  $\gamma_1$  and  $\gamma_4$ . Except for control  $\gamma_1$ , all the other active control are used, but considering the level of the thrusts,  $\gamma_3$  and  $\gamma_4$  are the most useful.

The following section will present an implementation of a  $(STPP)_2$  control strategy to our test-bed AUV.

#### 4 Experiments

The strategies computed from our STP algorithm are also implemented onto a test-bed AUV to further validate their implementability and efficiency. Here, we discuss the experimental set-up and highlight some advantages and limitations which we encounter.

Experiments are conducted twice each week in the diving well at the Duke Kahanamoku Aquatic Complex at the University of Hawaii. This diving well is a  $25m \times 25m$  pool with a depth of  $5m$ . This controlled environment allows us to focus on particular aspects of each control strategy or to isolate model parameters without the influence of external disturbances such as waves, other vehicles and complex currents. The downside to such a facility is that conventional sonar systems generate too much noise to function as an effective and accurate positioning solution. More significantly, in the implementation of our efficient trajectories, ODIN is often required to achieve large ( $> 15^\circ$ ) list angles which render the sonars useless for horizontal positioning.

We have yet to implement an accurate and cost effective on-board positioning system. To resolve this issue, experiments are video taped from the 10m diving platform. This gives us a near nadir view of ODIN's movements. Videos are saved and horizontal position is post processed for later analysis. This solution is able to determine ODIN's relative position within the pool to less than  $10cm$ . However, closed-loop feedback on horizontal position is not possible. Since our control strategies are directly based upon the vehicle model, this open loop framework does not hinder our implementation, and experimental results compare very well with theoretical predictions.

As noted throughout this paper, the control strategies we consider are for implementation onto an autonomous vehicle. For safety reasons, and in an effort to maximize the number of tests conducted each day, ODIN is tethered to the shore based command center. The tether connects to the top of ODIN and is routed down the backside of the sphere and attached to the bottom with the excess slack allowed to sink to the bottom of the pool. With this configuration, the strategies are run in autonomous mode, but real time data for orientation and depth are sent back to the operator throughout the experiment. A typical experiment begins with a closed-loop dive to  $1.5m$ . We allow the vehicle to stabilize with respect to depth and orientation, and then a signal is sent from the command center to begin the desired open-loop strategy.

Figure 6 shows the results of an experiment along with the 6 DOF control strategy applied. The applied control strategy is a  $(STPP)_2$  solution with thruster failure scenario  $\{2, 3\}$ ,  $c_T = 1.75$  and  $\chi_T = (5, 4, 1, 0, \dots, 0)$ . The experimental position and orientation evolution is displayed in solid line, while the theoretical evolution (based on our dynamic model) is displayed in dashed dotted line.

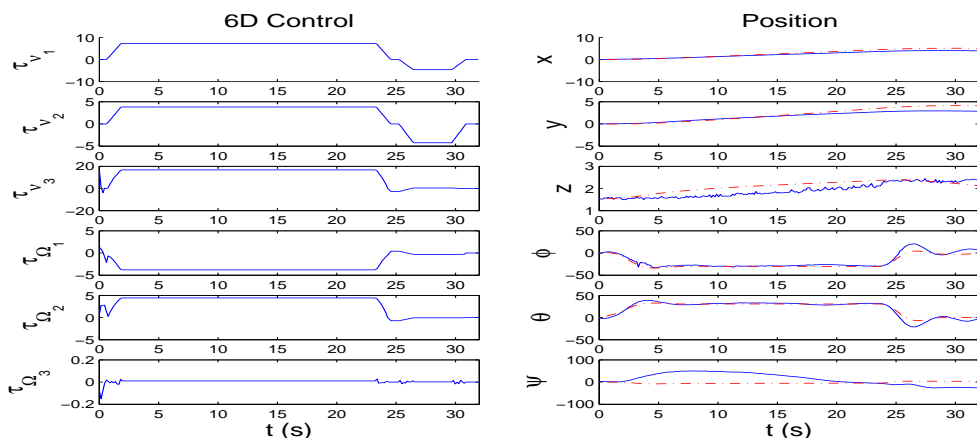


Fig.6:  $(STPP)_2$  6D control strategy for  $c_T = 1.75$  and failure of thrusters 2 and 3. Theoretical (dash dot) and experimental evolutions (solid) evolution of  $\eta$  are displayed.

As one can see on Figure 6, the experimental evolution follows extremely well the theoretical one for all the positions and orientations except for the yaw  $\psi$ . This discrepancy is not due to a poor approximation for the hydrodynamic model but to a lack of accuracy of our thrusters calibrations. Indeed, since we do not have any feedback on the thruster's output, it is not possible for us to directly observe and correct the calibrations. Thus, we cannot guarantee that when we ask a thruster, say  $\gamma_1$ , to deliver a given thrust

it is actually delivering exactly the demanded thrust. So we know that when we want to apply a surge and sway control with no yaw (that is  $\tau_{\Omega_3} = 0$ ), we inevitably get a *phantom* torque  $\tau_{\Omega}$ . This issue of *phantom thrust* is of course present for all the 6 DOF control components. However, the yaw is more sensitive than the other state because its dynamic do not have any restoring forces that would dampen the control inaccuracy. This discrepancy of the yaw evolution, implied that the AUV will not be orientated as expected and that the surge and sway will not match perfectly the theoretical evolution. However, we can see that while not being constant to zero, the yaw evolution does not explode and let the vehicle in the good general direction: there is no discrepancy superior than  $45^\circ$  and the average of the yaw is not far from  $0^\circ$ .

## 5 Conclusion

As seen in the two previous sections, the control strategies we built have the advantage of both being implementable on our test-bed AUV and efficient in terms of power consumption. Our theoretical model, though not perfect, is very accurate when considering the inherent difficulties implied by the medium the vehicle is evolving in. Concerning the minimum consumption criterion as well as the thruster failure scenarii, we only uncovered the top of the iceberg and will need to study thoroughly and rigorously the impact of various parameters such as buoyancy or final configuration. A central question to be answered is the one of the controllability that was only scratched in this paper. Concerning our theoretical model, in order to improve it we will need to work on a way to measure accurately the thrust applied by a thruster or just the rotational speed of the shafts. Once this is done, we will need to work out a well defined inverse problem to identify each and every parameters intervening in our model.

## 6 Acknowledgments

Research supported by NSF grant DMS-030641 and DMS-0608583 and partially supported by ONR grant N00014-03-1-0969, N00014-04-1-0751 and N00014-04-1-0751.

## References

- BERTRAM, V.; ALVAREZ, A. (2006), *Hydrodynamic aspects of AUV design*, 5<sup>th</sup> Int. Conf. Computer Applications and Information Technology in the Maritime Industries, Leiden
- BULLO, F.; LEWIS, A.D. (2004), *Geometric Control of Mechanical Systems Modeling, Analysis, and Design for Simple Mechanical Control Systems*, Springer-Verlag, New York-Heidelberg-Berlin, 49 in Texts in Applied Mathematics
- CHYBA, M.; HABERKORN, T.; SMITH, R.N.; WILKENS, G.R. (2007a), *Geometric Properties of Singular Extremals for a Submerged Rigid Body*, Preprint, University of Hawaii (<http://www.hawaii.edu/mchyba/publications/index.html>)
- CHYBA, M.; Haberkorn, T.; Smith, R.N.; Choi, S.K. (2007b), *Design and Implementation of Time Efficient Trajectories for Autonomous Underwater Vehicles*, IEEE Journal of Ocean Engineering, 2008.
- CHYBA, M.; Haberkorn, T.; Smith, R.N.; Choi, S.K. (2007c), *Autonomous Underwater Vehicles: Development and Implementation of Time and Energy Efficient Trajectories*, Ship Technology and Research, 2008.
- CHYBA, M.; Haberkorn, T.; Singh, S.B.; Smith, R.N.; Choi, S.K. (2008), *Increasing Underwater Vehicle Autonomy by Reducing Energy Consumption*, IEEE Journal of Ocean Engineering, submitted.
- FOSSEN, T.I. (1994), *Guidance and control of ocean vehicles*, Wiley, New York
- FOURER, R.; GAY, D.M.; KERNIGHAN, B.W. (1993), *AMPL: A Modeling Language for Mathematical Programming*, Duxbury Press, Brooks-Cole Publ.
- IMLAY, F.H. (1961), *The complete expressions for added mass of a rigid body moving in an ideal fluid*, Technical Report DTMB 1528

MACIVER, M.A.; FONTAINE, E.; BURDICK, J.W. (2004), *Designing future underwater vehicles: Principles and Mechanisms of the Weakly Electric Fish*, IEEE J. Oceanic Eng. 29/3

MOLNAR, L.; OMERDIC, E.; TOAL, D. (2005), *Hydrodynamic aspects of AUV design*, Ocean 2005 Europe IEEE Conf., Brest

PONTRYAGIN, L.S.; BOLTYANSKI, B.; GAMKRELIDZE, R.; MICHTCHENKO, E.(1962), *The Mathematical Theory of Optimal Processes* Interscience, New York

WAECHTER, A.; BIEGLER, L.T. (2006), *On the implementation of an interior-point filter-line search algorithm for large-scale nonlinear programming*, Research Report RC 23149, IBM T.J. Watson Research Center, Yorktown